Multi-axis Nanopositioning System for the Hard X-ray Split-Delay System at the LCLS

Hongliang Shi*, Diling Zhu
Linac Coherence Light Source, SLAC National Accelerator Laboratory
Menlo Park, CA 94025, U.S.A
Email: hshi2@slac.stanford.edu

INTRODUCTION

Modern optical laser technology has enjoyed great success thanks to the large variety of optical elements that are available to manipulate the beams with sub-wavelength precision. With the advent of several x-ray free electron laser facilities over the past decade[1-5], extension of many powerful optical laser techniques into the x-ray wavelength regime are being considered, where researchers face major technical challenges in the design and fabrication of systems that can serve as basic beam manipulation optical elements such as mirrors, lenses, gratings, filters, polarizers, beam splitters, delay lines, etc, due to the stringent requirement imposed by the Ångstrom scale wavelengths. Delay line for hard x-ray wavelengths in particular, was envisioned as early as the 1990s, based on perfect-crystal reflections. A particular application called split-pulse X-ray correlation spectroscopy was noted in the *First Experiment Document* of the Linac Coherence Light Source (LCLS) [6], as a rather unique technique that is able to capture atomic scale equilibrium dynamics of matter in the femto- and picosecond time scale.

A first effort to build a hard x-ray delay line by Roseker et al. adopted a single-photon-energy design [7], using thin silicon crystals as potential beam splitters. This system contained 8 crystals in total to achieve the beam splitting and recombination functionality. Silicon (333) reflection was chosen in a 90 degree diffraction geometry at 8.39 keV, such that the delay can be adjusted via a single linear translation stage. A later prototype system by Osaka et al. featured a pair of channelcuts serving as the fixed-delay branch, and used edge-polished silicon crystals to spatially split the beam [8]. In this case, silicon (220) reflection was chosen to provide larger bandwidth thus higher photon flux. These design changes greatly simplified the alignment procedure and the first observation of single-shot hard x-ray interference fringes were successfully achieved [9]. More recently, a new hard x-ray split-delay system was designed and constructed for the X-ray Correlation Spectroscopy (XCS) instrument at LCLS, with the goal of covering the whole hard x-ray photon energy range of LCLS, and reaching beyond the time delay value of 350 ps [10]. In this report we describe the design concept and the performance achieved at the early commissioning stage.

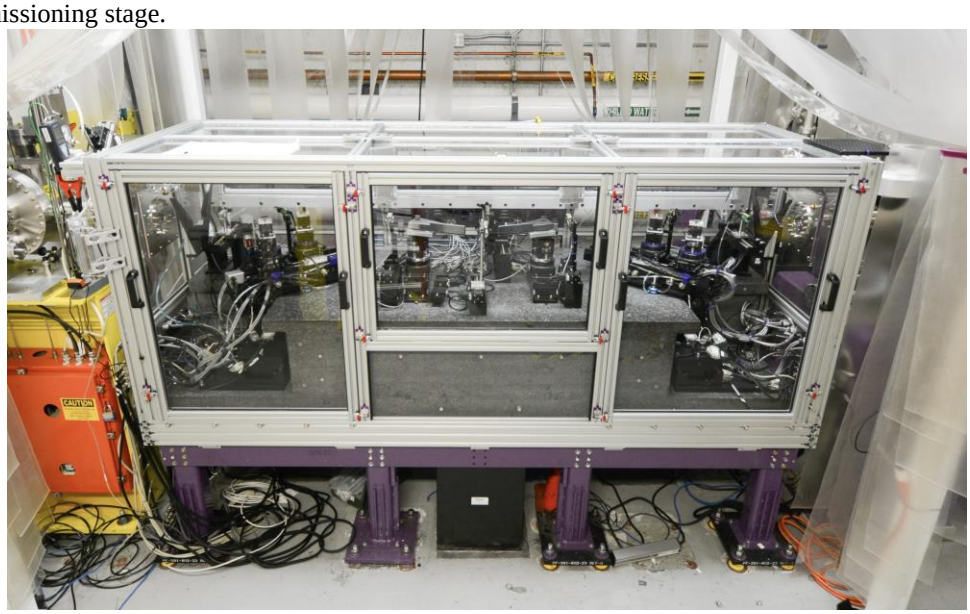

FIGURE 1. The hard x-ray split and delay system as installed in the downstream end of the x-ray transport tunnel just upstream of the XCS instrument.

This material is based upon work supported by the U.S. Department of Energy,
Office of Science, under Contract No. DE-AC02-76SF00515.

MOTION SYSTEM REQUIREMENT

The primary functionality of the hard x-ray split-delay (SD) optical system is to create two x-ray pulses from a single x-ray pulse, and introduce an adjustable time separation between the two pulses. For this particular implementation at the LCLS, the geometry is similar to the prototype system reported in [8]. However, horizontal scattering plane instead of vertical was chosen for the crystal reflections in anticipation of the vertically polarized hard x-ray undulator upgrade for LCLS-II. A photo of the completed system is shown in Fig. 1. The overall system schematic layout is shown in Fig. 2. Four silicon (220) crystals are symmetrically positioned in the delay-adjustable branch in the upper part. The fixed-delay branch consists of a pair of channelcut crystals in the lower part. For a given photon energy, at the Bragg angle, the additional beam path length taken by the channelcut branch is determined by the gap size thus fixed. On the other hand, for the delay-adjustable branch, the beam path length can be adjusted via linear translations of crystal 2 and 3 along the beam propagation direction that is denoted by the arrows L_1. In order to position the crystals with sufficient precision, a multi-axis motion system with micrometer and nanoradian precision was developed, which consists of primarily 4 motion stacks: tower 1 and 4 for the delay-adjustable branch, and tower 2 and 3 for the fixed-delay branch. Retractable beam diagnostics are positioned before and after each crystal reflection to allow system alignment.

The most challenging aspect for the mechanical system design of the split-delay delay system is the angular precision requirement for the delay-adjustable branch. First of all, sufficient global angular accuracy will be required to allow quick tuning of the transimitted photon energy of each branch. Since the rocking curve width for silicon (220) in the intended photon energy range is on the order of 10 – 20 microradians, this is within the performance level of commercial high precision rotation stages after a routine calibration procedure. In addition, another highly desired capability for conducting two-pulse experiments, is to be able to scan the time delay or photon energy without having to constantly re-optimize beam spatial overlap on the sample. For the case of LCLS, where the SD system is approximately 400 m downstream from the source, and 8 meters upstream of the XCS nominal sample location, when using the beamline compound refractive lenses with 3.3 meter focal length, in order to keep the two foci stable with repect to each other at a level of 1 micron full width (FW), the combined angular error of the optics needs to be on the order of ~150 nrad FW. For photon energy scans, this drove the decision to place a common rotation R_1 below R_2 and R_3, such that the upper assembly can be rotated as an 'artificial channelcut' that maintains the output beam position and angle for small energy ranges. For delay scans, however, such requirement of the corresponding yaw/pitch motion error for the linear motion L_1 is more than an order of magnitude beyond the state of the art of linear translational stages. In order to provide the required travel range of approximately 300 mm, and at the same time maintaining a relatively compact footprint of the system, a customized linear motion system featuring decoupled horizontal and vertical airbearings was designed and integrated into tower 1 and 4. Airbearing mechanism is chosen for its minimal parasitic angular motion as well as high degree of error repeatability. We describe the detailed implementation and bench level characterization in the next section.

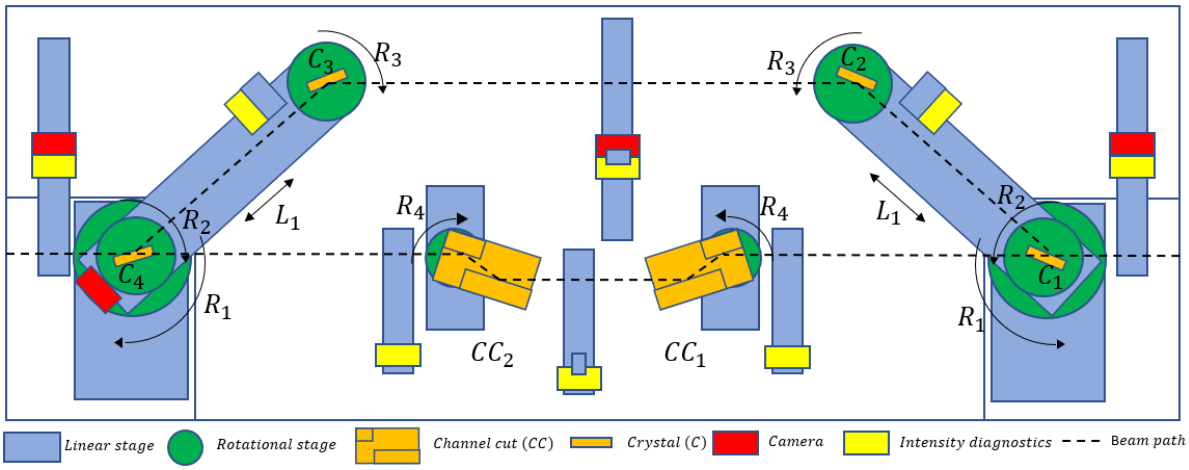

FIGURE 2. Schematic layout of motion system and diagnostics. The symbols illustrate the manipulation of crystal and channelcut to split and recombine the x-ray beam in the energy change and time delay.

MOTION SYSTEM DESIGN

For the delay adjustable branch, photon energy change of the system is accomplished by 6 rotational motion [11]: R_1, R_2, R_3 for both tower 1 and 4, as shown in Fig. 2. R_1 rotates to $2\theta_B$, while R_2 and R_3 both rotate to θ_B, where θ_B denotes the Bragg angle. In order to obtain both high resolution, stability and repeatability for these rotations at a reasonable speed and range, direct drive servo rotational stages were chosen. This avoids the motion backlashes from the gear driven rotation stages. On the other hand, while the gear driven stages generally provides a high torque, for the selection of servo motor stages, one needs to conisder not only the loading limit but also the rotational inertia. This is because the stage is actively controlled with an position feedback loop. In our design, Aerotech™ ANT95R stages were used for R_2 and R_3. A higher torque stage model APR150 was chosen for R_1, as shown in the photo in Fig. 3. The close-loop minimum step can both reach less than 50 nrad in our setup environment. After knowing inertia and resolution, one critical procedure in servo stage application is tuning the feedback control to achieve the desirable performance. In our application, a well tuned proportional–integral–derivative (PID) control algorithm is applied, such that R_2 and R_3 can reach a high stability with the jitter of rms 20 nrad and peak-to-peak 60 nrad. The crossover frequency is around 180 Hz.

One initial concern regarding the control stability of R_1 is that the total rotational inertia of the components above is varying as the distance between R_2 and R_3 changes during the delay time adjustement, even though the vertical loading on R_1 stays constant due to the de-coupled vertical air bearings. However, we found the optimal servo tuning parameters are relatively insensitive to L_1; thus there is no strong need for applying gain scaling. We have not fully investigated and optmized the dynamic stability of the system since currenlty the primary operation modes are step-scan rather than fly-scan. The settling time of R_1 was found to be within 300 millisecond with the current setting which was mainly optimized for in-position stability. The overall motion speed for larger range adjustments were all set at the 5mm/second and 2 degree/second scale.

As mentioned in the previous section, the time delay of the system is achieved by the two linear motions of L_1 on top of R_1. The design uses a felxure to decouple the motion in vertical and horizontal directions, the two translational motions perpendicular to the lead screw that drives the linear motion. As can be seen in Fig 3, the linear stage consists of a guide bar, a lead screw driving mechanism, a flexure for motion decoupling, carriage block, 3 round vacuum-loaded planar air bearings for vertical support, and 4 rectangular air bearings for sliding the outer crystal along the guide bar. The guide bar was used as the the linear motion constraint in the horizontal plane. The two vertical surfaces of the guide bar were lapped to 7 μm in parallelism and 3 μm in flatness. A high-stiffness zero-backlash stainless steel lead screw driven by a servo rotatory motor works as the driving mechanism. The lead screw is 14 mm in diameter to have a higher stiffness relative to the air bearings. A flexure block of aluminum 7075-T651 was used to decouple the parasitic displacement from the lead screw to the carriage block supporting the motion machanisms below crystal 2 and 3. It is a serial chain of two symmetrical 1DOF flexures of translational motion. In order to increase the compliance of the flexure, notch joints were modified with extended 2 mm neck length and 0.2 mm neck width. Moreover, thermal cycling of the flexure block was applied prior to EDM Wire cutting for stress relieving. The carriage attached to the flexure block was optimized in structure for both high in-plane rotational and translational stiffness, and minimal footprint size. The carriage block is supported by three vacuum-loaded round air bearings that are distributed symmetrically around the gravity center of the carriage block. The vacuum preload of the air bearing increases the system stiffness in the vertical direction, and also provides the option of stable landing of the airbearings for improved the stability when needed. The combination of these air bearings and the flexure block allows the granite surface to serve as the reference and decouple the out-of-plane angles of the guide bar. 4 rectangular planar air bearings were installed within the carriage block and symmetrically push against the polished side surfaces of the guide bar. With the 4 rectangular air bearings, the carriage block was designed with a 105 Hz natural frequency along R_1, which is higher than the main vibration excitation frequencies, eg. pump for vacuum-loaded air bearing. Finally, in order to improve the control performance, an absolute linear encoder was used to monitor the linear position, while a rotatory encoder on the motor was used in the velocity control loop, because the linear motion is driven by a rototory motor.

FIGURE 3. Motion tower design detail. Left: tower 1. Right: tower 2. (a) piezo *Z* stage, (b) piezo goniometer, (c) manual *XY* translation stages, (d) servo rotation stages, (e) servo air bearing linear stage with decoupled motion, (f) servo rotational stage with higher load capacity, (g) servo linear stage, (h) intensity monitors, (i) crystal 1 of the delay adjustable branch, with a polished upper edge, (j) vacuum pre-loaded planar air bearing that supports the crystal motion assembly for crystal 2, (k) large silicon channelcut with a gap size of 55 mm. (l) manual goniometer, (m) step motor linear stage for diagnostic insertion and removal.

In order to achieve system level accuracy and precision, installation and alignment are important. An AA grade granite table with 12 μm overall flatness was used to support the motion mechanics. The top surface was aligned to be parallel to the x-ray beam direction within 15 μrad. As the granite table as the reference plane, tower 1-4 are formed with stacking of single axis stages to create the multi-DOF motion. This type of topology creates a mechanism of serial chain. The alginment error of two adjacent axes will result in the systematic errors in each motion, some of which can not be calibrated or compensated. However, different from a parallel mechanism, eg. hexapod, a mechanism with the topology of serial chain directly stacks the systematic error of each motion axis so the accuracy of the multi-axis system is reduced. In order to achieve high accuracy, a feedback loop control is usually applied on the end effector of the serial chain, or an open loop control with complete kinematic modeling is derived and compensated on the systematic error of each axis. However, 6DOF feedback is hard to achieve with very high accuracy with such large motion stroke, eg. applying 6 interferometer beams. The complete kinematic modeling and compensation for such high precision is also hard to achieve with the limitation of the measurment tool accuracy, eg. laser tracker accuracy is around 25 μm. In order to reduce this multi-axis motion error of serial chain, we adopted shimming and precision adjustment screw, and made all the individual axes reference to the same granite table top surface with less than 100 μrad tolerance. Besides the shimming procedure, some stages were also used in the alignment procedure. As illustrated in Fig. 3, crystal 1 has a total of 8 DOF and 3 of them are redundent, which are 1 DOF for parking the tower into non operation mode, and 2DOF manual stage for aligning coaxis of R_1 and R_2 during installation. Of the 5 DOF actual motion, piezo goniometer and vertical z stage were used to align the top crystal to match the beam positions and propagation directions.

A photo of tower 2 which is part of the fixed-delay branch is shown in Fig. 3 on the right. The channelcut allignment only requires 5 DOF motion and we minimized the number of motorized axis to 2. The base linear motion was used to bring the short reflection surface of the channelcuts to the beam, or translate the crystal out of the way in the 'bypass' mode. Same Aerotech^{TM} ANT95R rotation stages were used here and synchronous rotation between the two R_4 can be performed during an energy scan of the fixed-delay branch. The manual stages were used to bring the crystal surface to the center of rotation, and for compensating crystal miscut.

SYSTEM PERFORMANCE

Early commissioning of the system took place in late 2017. With the assistance of intensity monitors positioned in-between every crystal, alignment of the whole system can be quickly completed and re-evaluated during the experiment. The overall system photon throughput was evaluated using a diamond (111) monochromator upstream as the input, and was estimated to be between 50-70% of the calculated value. Focal spot size below 2 μm was achieved from both branches, using the XCS beamline beryllium compound refractive lens setup with a focal length of ~ 3.3 m. The temporal overlap can be established by maiximizing the contrast of the interference fringes when crossing the two unfocused half beams with a small angle. Fig. 4(a) is an example of the interference fringes observed on a scintillator screen ~15 meters down stream of the SD system. We were also able to achieve a rather balanced branching ratio, as shown in Fig. 4(b), where the measured pulse energy from the two branches show a relatively clean correlation. The remaining spread of the correlation can be mostly attributed to beam spatial jitter and the spatial splitting mechanism from the polished silicon edge crystal.

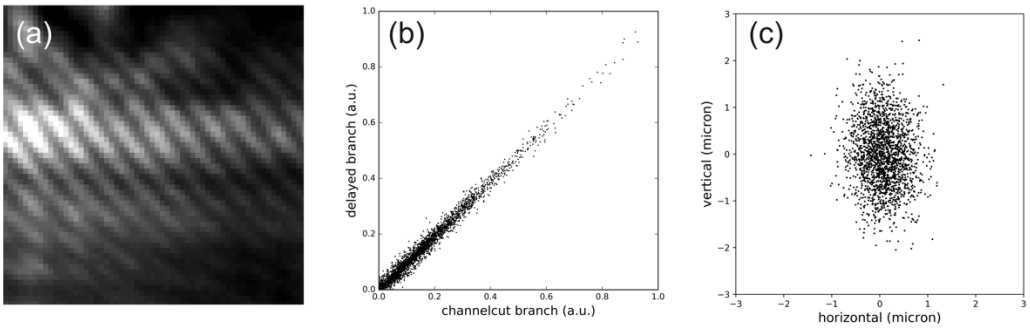

Figure 4, (a) A typical interference fringe pattern seen at time zero when crossing the two output beams at a small angle. (b) pulse-to-pulse correlation between pulse intensities from the two branches. (c) a scattered plot showing relative focal position stability between the two branches.

The central question regarding the stability of the system is how well the two foci overlap with each other shot-to-shot. This was evaluated using a high-resolution scintillator-based imaging system. The relative positional jitter was found to be ~0.3 μm (rms) in the horizontal, and ~0.6 μm (rms) in the vertical, as shown in Fig. 4(c). This approximately translates to total angular fluctuations of ~ 50 nrad (rms) for the crystal optics in the scattering plane between the two branches. This is consistent with the encoder readout of the 4 upper rotation stages which are all in the range of 20-30 nrad. The observed vertical jitter is larger partially due to imperfection of the channelcut surface and the focal shape variation. The vertical jitter is expected to improve after repolishing the channel surfaces. The relative positional drift was found to be on the order of 1 micron per hour without any active environment control. The alcove area where the system was installed showed temperature stability of ± 0.1 degree Celsius about half a day after the closure of the tunnel. The plan is to further improve this by controlling the temperature of the helium that is being purged into the enclosure. Additional reconfiguration of the service loop is also expected to reduce the level of vibration coupling between the enclosure and the stages.

As discussed earlier, the primary reason for choosing an air bearing based linear motion system for delay adjustment is to achieve a high level of motion repeatability such that the remaining systematic motion errors can be corrected via a look-up table. A preliminary study was performed looking at the trajectory of the focused beam on a scintillator screen while repeating delay scans over a range of 20 ps. We found that while the delay branch beam position can be changing by as much as 10-20 μm, the position repeatability across the whole range is within 2 μm peak-to-peak. This 'pointing wobble' during the delay motion can thus be compensated by small angular corrections in both pitch and roll of crystal 4.

CONCLUSION AND OUTLOOK

In conclusion, a new hard x-ray split-delay system was recently developed, built, and commissioned for the XCS instrument at the LCLS. This system has adopted two customized air-bearing-based linear motion mechanism for the delay adjustment. The first experience deploying this system for user experiment was largely positive. The

system alignment was quick and consistent thanks to the fully-encoded servo and piezo motion system. The intensity diagnostics between the crystals provided crucial online monitoring of the whole system alignment and throughput. The linear motion largely worked as expected and we anticipate the angular error compensation mechanism to be fully implemented in the coming months, such that beam position can be maintained at the repeatability level during a delay scan. An interferometer-based crystal angle monitoring and active feedback system is also being considered such as the ones used in [12, 13]. Cable routing needs to be optimized in service loop to increase the system repeatability. A linear-motor-based air bearing stage is under development to improve the performance of the lead screw driving mechanism.

ACKNOWLEDGMENT

The reported work is conducted at the Linac Coherent Light Source (LCLS), SLAC National Accelerator Laboratory, which is supported by the U.S. Department of Energy, Office of Science, Office of Basic Energy Sciences under Contract No. DE-AC02-76SF00515

REFERENCES

1. P. Emma, *et al.*, Nat. Photonics **4**, 641 (2010).
2. H. Tanaka, *et al.*, Nature Photonics **6**, 540 (2012).
3. H.-S. Kang, et al., Nature Photonics **11**, 708 (2017).
4. C. Milne, *et al.*, Applied Science, **7**, 720, (2017).
5. H. Weise, *et al.*, Proceedings of 38th International Free Electron Laser Conference, **MOC03**, 9, (2017).
6. G. Shenoy, *et al.*, *LCLS: The First Experiments* (2010).
7. W. Roseker *et al.*, Optics Letters, **24**, 1768-1770 (2009).
8. T. Osaka, *et al.*, Optics Express, **24**, 9187-9201 (2016).
9. T. Osaka, *et al.*, Journal of Synchrotron Radiation, (2017).
10. D. Zhu, *et al.*, Proceedings of SPIE **10237**, 10237 (2017).
11. H. Shi, *et al.*, Proceedings of ASME IDETC/CIE, V05BT08A031 (2017).
12. S. Rolling, *et al.*, Proceeding of SPIE **92100**, 92100B (2014).
13. W. Lu, *et al.*, Review of Scientific Instrument **89**, 063121 (2018).